THE JOURNAL OF PHYSICAL CHEMISTRY C

Article

Cite This: J. Phys. Chem. C 2018, 122, 3638−3647

pubs.acs.org/JPCC

Diffusion of Water and Electrolytes in Mesoporous Silica with a Wide Range of Pore Sizes

Diana C. Martínez Casillas,[†] M. Paula Longinotti,*[,†] Mariano M. Bruno,[‡,⊥] Fabián Vaca Chávez,[§] Rodolfo H. Acosta,[§] and Horacio R. Corti*[,†,‡]

[†]Instituto de Química Física de los Materiales, Medio Ambiente y Energía (INQUIMAE-CONICET), Facultad de Ciencias Exactas y Naturales, Universidad de Buenos Aires, Pabellón II, Ciudad Universitaria, C1428EGA Buenos Aires, Argentina

[‡]Departamento de Física de la Materia Condensada, Comisión Nacional de Energía Atómica, Avda. General Paz 1499, B1650WAB, San Martín, Buenos Aires, Argentina

[§]Facultad de Matemática, Astronomía y Física, Universidad Nacional de Córdoba, Medina Allende s/n, Ciudad Universitaria, X5016LAE Córdoba, Argentina & IFEG-CONICET

Supporting Information

ABSTRACT: The diffusion of alkaline chlorides (LiCl, KCl, and CsCl) and water in mesoporous silica samples with pore sizes covering the range from micropores (2 nm) up to mesopores larger than 30 nm have been measured by resorting to a simple diffusional technique in the case of electrolytes and ^{1}H NMR in the case of water. The morphology of the silica samples varies from a microporous structure, an interconnected network of pores, and typical mesoporous materials with ink-bottle pores, with increasing pore size. The release of electrolytes from the silica as a function of time exhibits two differentiated regimes, at short and long times, which correlates quite well with the size of the pores and that of necks of the pores, respectively. The diffusion of water inside the pores follows the same trend with pore size that the diffusion of electrolytes, indicating a coupling between the ions and water diffusional mobilities. The tortuosity effect on the diffusion of all studied electrolytes and water shows a monotonic slight increase with decreasing diameter for pores larger than 5 nm, while the tortuosity factor increases markedly for smaller pores. In microporous and mesoporous silica with pore sizes below 10 nm, the tortuosity factor of Li^+ ion is much larger than those for K^+ and Cs^+ ions, since its diffusion is hindered by a stronger electrostatic interaction with the ionizable silanol groups on the pore wall; and also larger than that for water diffusion which it is retarded by a weaker hydrogen bond interaction with the silanol groups. The differences in tortuosity factors among alkaline chlorides and water become negligible for pore sizes larger than 10 nm. The spin−lattice relaxation time measurements of ^{1}H-water and Li^+ ions confirm this behavior.

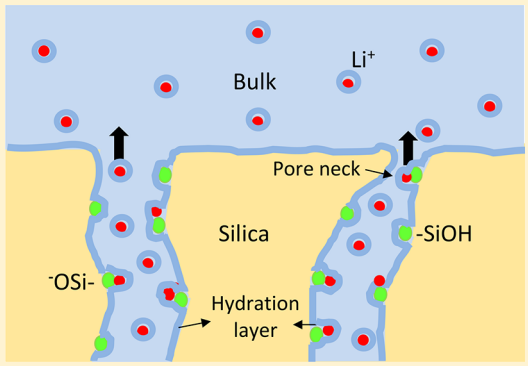

INTRODUCTION

The liquid phase diffusion of water and electrolytes in natural and synthetic mesoporous materials is of great interest for many practical applications, such as nanofluidics, desalinization, catalysis, batteries, and supercapacitors, among others.

Water diffusion in nanometric sized pores has been widely studied in the literature by NMR[1−3] and neutron scattering[3−5] experiments performed mainly in ordered nanoporous hydrophilic silica, such as MCM-41, and SBA-15. Molecular dynamic simulations also provided insight on the structure and dynamics of water in SiO_2 and TiO_2 nanopores.[6−13] For instance, Renou et al.[11,12] observed that the local organization of water in aqueous NaCl solutions confined in hydrophilic uncharged silica nanopores (1.2 nm in diameter) is mainly determined by the pore surface, while ion−water interactions are responsible for the water structure in the center of the pore. More interesting, the density of the water layer close to the surface increases with respect to the bulk water, and the exclusion of Na^+ and Cl^- ions from the pore is very important (80 and 90% with respect to the reservoir ion density, depending on the model adopted to describe the ion−water interactions). Other molecular dynamics simulations reveal that for pore diameters larger than 2 nm, the pore surface is covered with up to three monolayers of density-layered water, while bulk-like water, without density layering, exists at the center of the pore.[6,12,13] However, the reported density profiles of the layered and bulk-like regions differ among simulations and, in some cases, from experimental neutron diffraction results.[14]

Dynamical properties of ions confined in functionalized silica pores with hydrophobic and hydrophilic uncharged surfaces have been analyzed using molecular dynamics simulations.[7,8,11−13,15,16] Striolo et al.[7,8] analyzed the diffusion of

Received: November 23, 2017
Revised: January 16, 2018
Published: January 16, 2018

DOI: 10.1021/acs.jpcc.7b11555
J. Phys. Chem. C 2018, 122, 3638−3647

water, Na^+, Cs^+, and Cl^- ions in silica nanopores 1 nm in diameter. The results show evidence of ion-specific properties that depend on ion-surface, ion−water, and only in some cases, on ion−ion correlations. Besides, the authors noticed that the degree of protonation of the silanol surface groups strongly affects the structure, distribution, and the dynamic behavior of confined water and electrolytes. For instance, Cl^- ions adsorb on the surface at large degrees of protonation, independently of the cation type. On the other hand, Na^+ ions occupy different positions within the pore depending on the protonation degree, while Cs^+ ions mainly remain in the center of the pore, no matter the protonation degree. As a result of this, Cs^+ diffusion is faster than that of the Na^+ ion, and the diffusion coefficients in the pore are approximately 1 order of magnitude smaller than those reported in bulk. Contrarily, Videla et al.,[13] did not observe large modifications of the Na^+ and Cl^- diffusion coefficients in neutral pores of 2 and 3.75 nm in diameter compared to the bulk values. However, the electrical conductivity of the electrolyte solutions exhibited important reductions which could be explained using simple geometrical considerations, taking into account the reduction in the volume occupied by the electrolyte solution given by the fact that the pore walls are exclusively coated with water.

In contrast, experimental results on the diffusion of ions in aqueous electrolytes confined within mesoporous silica are scarce.[17−19] Takahashi et al.[17] analyzed the pore size effect on the diffusion of aqueous nickel nitrate in mesoporous silica by UV−visible spectroscopy and observed that, for materials with pore diameters larger than 5 nm, the tortuosity was close to unity and independent of the pore size, while it increases rapidly with decreasing pore diameter because of the reduction in the microscopic mobility of the ions due to their interactions with the wall. A similar trend has been reported by Kunetz and Hench[18] for the diffusion of chromium nitrate in porous sol−gel silica monoliths, with tortuosity increasing suddenly in pores smaller than 3 nm. Koone et al.[19] reported diffusion coefficients for Er^{3+} ions in the 4.2 nm diameter pores of a sol−gel glass without discussion about confinement effects.

The mobility of ions confined in nanopores is expected to be determined by ion−surface interactions and by the structure and mobility of water, which depends on the nature of the water−surface interactions. However, little attention has been paid in the literature to the experimental study of the coupling of ionic and water diffusion in mesoporous materials over a wide range of pore sizes. For this reason, the main goal of our study is the analysis of possible correlations between ion and water (solvent) diffusion properties confined in mesoporous silica.

In this work, we studied the diffusion of aqueous alkali chlorides electrolytes (LiCl, KCl, and CsCl) in silica mesoporous materials with average pore diameters between 2 and 58 nm by resorting to the measurement of the electrical conductivity of well stirred water in contact with macroscopic mesoporous samples filled with aqueous electrolyte solutions. This technique allows studying the diffusion of a wide variety of ionic solutes. The diffusion coefficients of water and the spin−lattice relaxation times for water's protons and Li^+ ions within the mesoporous silica were determined by ^1H and ^7Li NMR techniques. The results allow us to have an insight on the coupling between water and salt diffusion, and the tortuosity or confinement effect as a function of the pore size of the silica samples.

EXPERIMENTAL SECTION

Materials. Commercial silica spheres, 1−4 mm in diameter (CARIACT Q), with five different nominal nanometric pore sizes (namely 3, 6, 10, 15, and 30 nm) were acquired from Fuji Silysia Chemical Ltd.,[20] and used after vacuum drying at 120 °C overnight. We denominate these samples as Q3, Q6, Q10, Q15, and Q30, where the numbers indicate the nominal pore sizes. LiCl, KCl, and CsCl were purchased from Merck and vacuum-dried overnight at 120 °C prior use. Buffers of pH 4, 7, and 10 were from Bio Pack. All the solutions were prepared using Milli-q water.

Filling of the Mesoporous Samples with Electrolyte Aqueous Solutions. The silica spheres were filled up with 0.1 M MCl (with M = Li, K, or Cs) aqueous solutions according to the following protocol. Silica spheres (between 3 and 5), previously weighted, were placed in a tube containing 1 cm^3 of aqueous MCl solution. The solution inside the tube was frozen with liquid nitrogen and the tube was connected to a vacuum line to remove the air. Then, the valve connecting the tube to the vacuum was closed and the solution was melted, allowing the air, dissolved in the solution and filling the silica pores, to occupy the free volume. Once the equilibrium was reached, the solution was frozen again and connected to the vacuum to remove the air. This process was repeated several times until no bubbles were observed to get out from the silica spheres, indicating that pores were free from air, although some sorbed water could remain onto the surface of the pores. Once the solution is melted by the last time, the valve was opened to the atmosphere to force the solution filling the pores. Finally, the spheres were removed from the solution, dried with tissue paper to remove the solution wetting the external surface, weighed to determine the mass of solution inside the samples, and kept in closed vessels with 0.1 M alkaline chloride solution prior to the measurements. The equilibration of the samples with a large amount of external solution during a long time assures that the internal concentration in the pores reaches equilibrium with external one, even in case that hydration water was trapped inside the pores during the filling up process.

Mesoporous Silica Chracterization. The surface of the spheres was characterized by Scannig Electronic Microscopy (SEM) in a Carl Zeiss NTS-SUPRA 40 operated at 3 kV (Center of Advanced Microscopy, University of Buenos Aires).

The specific surface area of the spheres was determined from the nitrogen adsorption isotherm at 77 K measured with a Micromeritics ASAP 2020, using the Brunauer−Emmet−Teller (BET) equation. For the characterization of all silica samples, adsorption and desorption isotherms were analyzed with the Barrett, Joyner, and Halenda (BJH) model,[21] where the thickness of the adsorbed layer was determined with the equation given by Broekhoff−de Boer (BdB).[22]

The density charge on the walls of the mesoporous silica was determined by potentiometric titration starting from the alkaline side, following the procedure reported by Sonnefeld et al.,[23,24] and also starting from the acid side, according to the procedure by Dove and Craven,[25] and Salis et al.[26] The spheres of silica were powdered, to increase the exposed area, and vacuum-dried overnight at 120 °C. For the alkaline titration, a known mass of powdered silica was immersed in 32 cm^3 of a 0.1 M LiCl solution bubbled with N_2. This suspension was equilibrated for 16 h under stirring, followed by the addition of 20 μL of 0.1 M NaOH, in order to raise the pH around 7, and the suspension was left to equilibrate for approximately 1 h

DOI: 10.1021/acs.jpcc.7b11555
J. Phys. Chem. C 2018, 122, 3638−3647

prior to the titration. The solution was titrated drop by drop with 0.1 M HCl, and the pH was recorded as a function of the titrant mass using a pH/Ion meter HI 2211 (Hanna Instruments), taking care that it remained constant for at least 5 min after each HCl addition. For the acid titration, the powered silica sample, immersed in 32 cm^3 of 0.1 M LiCl, was equilibrated overnight under stirring. Then a concentrated aqueous HCl solution was added to obtain a pH < 2, and after 1 h was titrated with 0.1 M NaOH up to pH ∼ 8.5.

Using the potentiometric titration data, the surface charge density, σ_{pH}, of the material was calculated, as a function of pH, according to the following equation:[26]

$$\sigma_{pH} = \frac{F\Delta n_{pH}}{mS_{BET}} \quad (1)$$

Here F is the Faraday constant, Δn_{pH} is the difference between the moles of titrant used for the titration of the blank (HCl + LiCl solution without silica spheres) and those used for the titration of the sample at a same value of pH, S_{BET} is the surface area determined through the BET method, and m is the sample mass.

Diffusion of Electrolytes. In order to study the diffusion of LiCl, KCl, and CsCl through the silica nanopores, the silica spheres were filled with 0.1 M of the corresponding electrolyte aqueous solution using the procedure described in the previous section. The pH of the filling solution was adjusted by small additions of HCl or NaOH (0.1 M) and measured with the pH meter mentioned above. An airtight glass conductivity cell with a mixing bulb and platinized platinum electrodes was used to determine the concentration of the electrolyte released from the silica spheres in pure water as a function of time. The time evolution of the electrolyte concentration was obtained from the specific conductivity of the solution, $\kappa(t)$, and the molar conductivity, Λ, of the salts in water, by assuming that its concentration is low enough, in such a way that the Onsager limiting law holds. Thus

$$c(t) = \frac{\kappa(t)}{\Lambda[c(t)]} = \frac{\kappa(t)}{(\Lambda^0 - Sc(t)^{1/2})} \quad (2)$$

where S is the Onsager slope in water and Λ^o is the infinite dilution molar conductivity of the electrolyte.[27] For the calculation of the specific conductivity, the cell constant was determined by measuring the resistance of the cell in a KCl aqueous solution of known specific conductivity.[28] Resistance measurements were performed with an LCR meter (GW Instek). All measurements were performed at 298.15 ± 0.05 K. The concentration as a function of time was determined following an iterative procedure, fixing initially $\Lambda=\Lambda^0$ in eq 2, and repeating the calculation until convergence was reached.

In order to calculate the apparent diffusion coefficient, D_p, of the electrolyte in the porous media a model corresponding to the desorption of a sphere with radius (a) in an infinitum bath, was used[29,30]

$$\frac{c(t)}{c_f} = 1 - \frac{6}{\pi^2}\sum_{n=1}^{\infty}\frac{1}{n^2}\exp\left(\frac{-\pi^2 n^2 D_p t}{a^2}\right) \quad (3)$$

where $c(t)$ is the concentration of electrolyte in the solution obtained from Eqn. 2, c_f is the final concentration of the electrolyte in the solution, estimated from the mass of electrolyte in the spheres (considering a partition constant equal to 1) and the amount of pure water in the conductivity cell, and a is the radius of the sphere. In our case, where more than one sphere was used in each measurement, spheres of equal radii were chosen for the measurements.

Equation 3 represents the diffusion of a solute from a sphere in an infinite bath. In this work the bath where diffusion occurs is not infinite. However, the ratio between the volume of the bulk solution and that of the spheres is around 350; being this number big enough to ensure that eq 3 gives a good approximation of the electrolyte concentration time dependence.

At long times ($D_p t/a^2 > 0.05$), the first term of the series in eq 3 sufficiently estimates the desorption times and the corresponding fluxes. Thus, D_p/a^2 can be determined by plotting $\ln[(1 - c(t)/c_f)(\pi^2/6)]$ vs. t.

At short times ($D_p t/a^2 < 0.15$), $c(t)$ can be approximated by the following expression:[29,30]

$$\frac{c(t)}{c_f} = 6\sqrt{\frac{D_p t}{\pi a^2}} - 3\frac{D_p t}{a^2} \quad (4)$$

being the second term of eq 4 negligible for $D_p t/a^2 < 0.01$. In this work, we calculated D_p using the long and short times approximations, that is for $D_p t/a^2$ larger than 0.05 and smaller than 0.15, respectively. The difference in the results obtained with both approximations will be analyzed in the Results, considering the coexistence of regular pores with ink-bottle type pores, where diffusion can be limited either by the size of the pores or that of the necks.

NMR Experiments: Diffusion and Spin−Lattice Relaxation Time. Water diffusion coefficient, D_p, and spin−lattice relaxation time, T_1, measurements were carried out for ^{1}H with a PM5 NMR-MOUSE (Mobile Surface Explorer) from Magritek GmbH, with a magnetic field corresponding to ^{1}H frequency of 20.3 MHz and a static magnetic field gradient G_0 = 23.5 $T.m^{-1}$. The diffusion coefficient was obtained using a stimulated echo pulse sequence and the detection was carried out using a Carr−Purcell−Meiboom−Gill (CPMG) sequence[31,32] with an echo time of 50 μs and acquisition of 150 echoes in order to improve sensitivity. The signal decay due to diffusion, neglecting the influence of relaxation, in the presence of a static magnetic field is[33]

$$\frac{s(\Delta)}{S_0} = \exp\left(-\gamma^2 G_0^{\,2}\tau_1^{\,2}\left(\tau_2 + \frac{2}{3}\tau_1\right)D\right) \quad (5)$$

where D is the diffusion coefficient, γ is the proton gyromagnetic ratio, τ_1 is the stimulated echo time, which was varied logarithmically in 50 steps from 15 to 300 μs, and τ_2 = 1 ms is the diffusion time. Measurements were carried out at 298 K for five fully saturated spheres for each pore size system and repeated three independent times. The diffusion coefficients were determined, with a dispersion of 5%, by using eq 5.

The ^{7}Li spin−lattice relaxation times were measured using saturation recovery pulse sequence on a Bruker Avance II 300 spectrometer operating at 116.6 MHz.

RESULTS AND DISCUSSION

Morphology and Pore Size Distribution (PSD) of the Mesoporous Silica Samples. The CARIACT Q samples are widely used as catalysts supports,[34−36] and it is assumed that the pore morphology is complex, being formed by an interconnected network of pores having a random length distribution. The surface of the spheres was characterized by

DOI: 10.1021/acs.jpcc.7b11555
J. Phys. Chem. C 2018, 122, 3638−3647

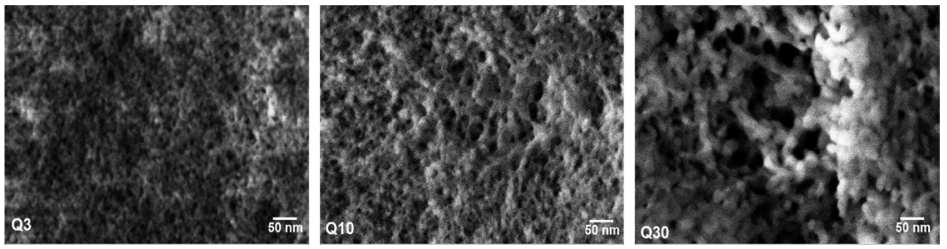

Figure 1. SEM micrographs of the surface of the CARIACT silica spheres: Q3 (left), Q10 (center), Q30 (right). Magnification 400 000×.

SEM, and the presence of randomly distributed pores can be observed in Figure 1 for the samples Q3, Q10, and Q30.

Figure 2 shows the BET N_2 adsorption and desorption isotherms. All samples show hysteresis loops characteristic of

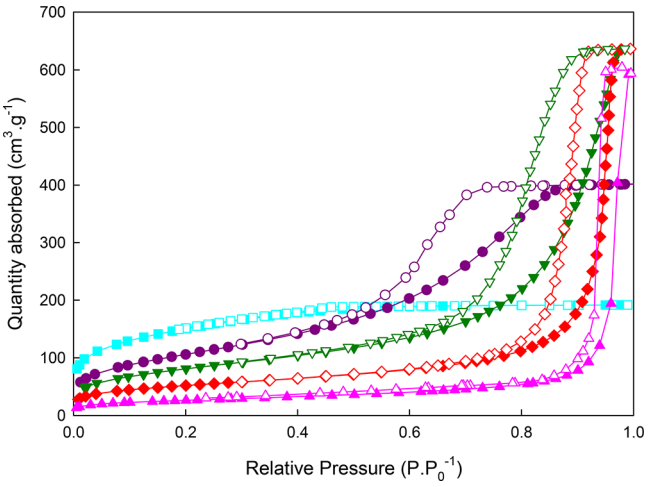

Figure 2. N_2 sorption isotherms for (blue ■) Q3, (purple ●) Q6, (green ▼) Q10, (red ◆) Q15, and (pink ▲) Q30 samples. Filled symbols correspond to the adsorption isotherms and open symbols to the desorption ones.

mesoporous materials, except in the case of sample Q3. In this sample, a higher steep uptake at low relative pressures, characteristic of Ib isotherms, can be observed indicating an important micropore contribution.[37] Samples Q6, Q10, Q15, and Q30 show an isotherm type IV with a H2(b) hysteresis loop, corresponding to materials that exhibit pore networks with ink-bottle shape pores.[38,39]

Several authors have reported that in samples with H2(b) hysteresis loops, and pores with necks or entrances bellow ∼5 nm, N_2 desorption can occur via cavitation, giving misleading results.[40−42] Q6 samples shows H2(b) hysteresis type, but the stepper desorption branch occurs at high relative pressure ($p/p^0 \approx 0.7$). This results would indicate that pore blocking/percolation is the dominant mechanism of evaporation, and neck information can be obtained from this branch.[42−44] Thus, from the PSD (desorption branch) an average neck size of 5.5 ± 1.0 nm can be estimated for the Q6 sample. Similar results were found for samples Q10, Q15, and Q30, whose estimated neck sizes are approximately half of the pore size.

Figure 3a and 3b show the pore size distributions (PSD), calculated with the BJH model, using the desorption and adsorption branches, respectively. It can be considered that the diameter of the pores can be obtained from the adsorption branch, while the desorption branch gives the diameter of the pore necks.[37] Table 1 shows, for the different silica samples, the

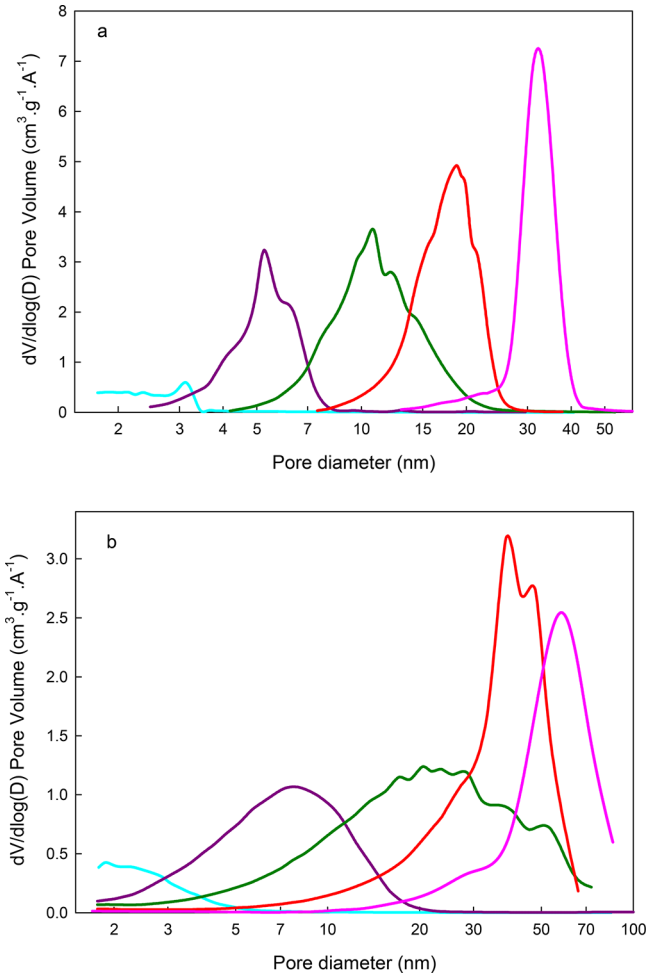

Figure 3. Pore size distributions obtained from the desorption and adsorption isotherms (a and b, respectively) for the silica mesoporous samples. The colors used in these plots are the same as in Figure 2.

average pore and neck diameters, along with the pore volume, specific surface area, and porosity. Porosity was calculated as $\varepsilon = V_p/(V_p + 1/\rho_{silica})$, where V_p is the pore volume determined from the BET measurements at $p/p^0 = 0.99$, and $\rho_{silica} = 2.1$ g·cm^{-3} is a mean value for the density of amorphous silica reported in literature, which ranges between 2.0 and 2.2 g·cm^{-3}. Average pore/neck sizes were determined by the position of the maximum in the PSD. In the case of sample Q3 the pore diameter can be considered to be extended around 2 ± 1 nm, involving micropore sizes. In this case, the PSD for the adsorption and desorption branches are very similar, as expected for a microporous sample where hysteresis loop is almost absent. The desorption branch yields a local maximum around 3 nm, which is probably an artifact due to the

DOI: 10.1021/acs.jpcc.7b11555
J. Phys. Chem. C 2018, 122, 3638−3647

Table 1. Pore Diameter (d_{pore}), Neck Diameter (d_{neck}), Pore Volume (V_p), Specific Surface Area (SA), and Porosity (ε) of the Mesoporous Silica Samples

sample	d_{pore} (nm)	d_{neck} (nm)	V_p ($cm^{-3}·g^{-1}$)	SA ($m^2·g^{-1}$)	ε	ref
Q3	2[a]	2[a]	0.29	540	0.38	this work
	3.0		0.3	550		20
Q6	8.0	5.5[a]	0.62	391	0.57	this work
	6.0		0.6	450		20
	6.9		0.62	359		34
Q10	20.4	10.6	1.00	297	0.68	this work
	10.0		1.0	300		20
	13.9		1.06	303		34
	17.8		1.32	284		35
Q15	38.3	18.8	0.98	188	0.67	this work
	15.0		1.0	200		20
	19.6		1.02	208		34
Q30	57.7	31.3	0.91	95	0.66	this work
	30.0		1.0	100		20
	25.0		0.70	112		34

[a]The d_{pore} values informed correspond to an extended range of ±1 nm

desorption process via cavitation that is characteristic for ink-bottle pores with small necks. Thus, for this sample two different pore sizes, for pore and neck, cannot be calculated. The PSD is given only above 1.7 nm due to the fact that Kelvin's equation is not valid for pores smaller than this value; however, an important contribution of micropores can be observed from the N_2 isotherm. This can be confirmed by the fact that the total volume is larger than the mesoporous volume. For the other samples pore and neck diameters can be well differentiated.

The values of the parameters reported in Table 1 follow the trend expected with the pore size, that is, the pore volume, and porosity increase with pore size, reaching almost constant values for pores with nominal diameters above around 10 nm. Table 1 also includes data reported by other authors,[20,34,35] where pore diameters for CARIACT Q samples are informed. These data do not indicate whether those values were obtained from the desorption or adsorption branches. However, compared with our results, it can be speculated that they were obtained from the desorption branches.

Surface Charge Density. The pore wall of mesoporous silica is expected to be covered by neutral silanol groups (−SiOH) that can dissociate or protonate depending on the pH of the media inside the pore. Sonnefeld et al.[24] have analyzed the surface charge density of Aerosil OX 50 (Degussa) spherical silica particles, with particle size much smaller than our samples, and BET superficial area of 50 $m^2·g^{-1}$. They obtained an isoelectric point, pH_{iso} = 2.4, and a dissociation constant for the silanol group corresponding to pK_d = 6.37. Sahai and Sverjensky[45] analyzed titration data of Aerosil (Degussa), and pyrogenic CAB-O-SIL silica, and reported pH_{iso} = 3.5, and pK_d = 7.7. Thus, it is expected that the surface negative charge density of mesoporous silica increases with pH, and becomes important at pH > 7.

Figure 4 shows our results obtained for sample Q30 as a function of pH, in the range between pH = 2 and pH = 8.5. We have chosen the sample with larger pores (Q30) for the titration because the diffusion of the reagents between the sample and the solution would be much faster that in the Q3 sample, which is expected to have the same surface chemistry that Q30, although some effect of the pore size on the protonation equilibria of the silanol groups cannot be discarded

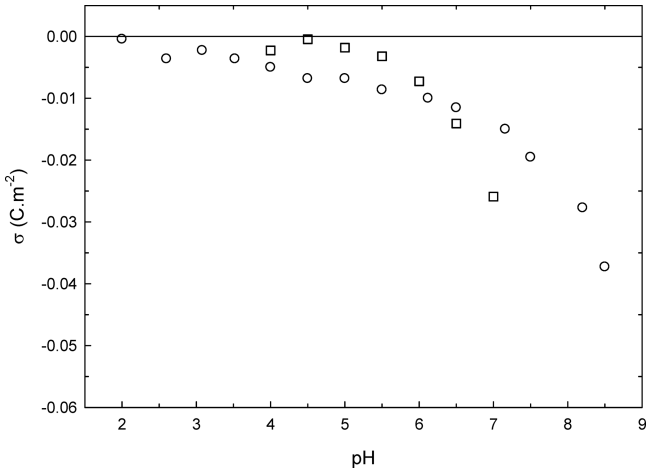

Figure 4. Surface charge density as a function of pH for CARIACT Q30 determined in this work for LiCl 0.1 M with alkali titration (○) and acid titration.

(see Supporting Information for a comparison of our surface charge density as a function of pH with other porous silica materials with different pore size).

It is observed that the surface charge density is very low (below 0.01 $C·m^{-2}$ for both titrations) in the range 4 < pH < 6, and starts to increases at pH > 6. It should be noted that a surface charge density of 0.01 $C·m^{-2}$ in the Q3 sample, with a pore diameter around 2 nm, corresponds approximately to an elementary charge each 16 nm, while for Q30 sample, considering a pore of 58 nm diameter, this charge density implies an elementary charge every 4 nm.

Figure S1 (Supporting Information) also shows the surface charge density as a function of pH for data reported by Sonnenfeld et al.,[23] Dove and Craven,[25] Salis et al.[26] and Sahai and Sverjensky[45] for different silica samples. It is clear that the magnitude of the negative charge on the surface depends on the type and concentration of the electrolyte in equilibrium with the sample, increasing with increasing electrolyte concentration, and following the trend: LiCl < NaCl < KCl < CsCl. According to Salis et al.,[26] this order is determined by a combination of ion-surface dispersion interactions and ion hydration. Sahai and Sverjensjy[45] used a triple-layer model to explain the

DOI: 10.1021/acs.jpcc.7b11555
J. Phys. Chem. C 2018, 122, 3638−3647

concentration and cation dependence of the titration curves of several oxides, including silica. They observed that the complex formation constant for the process $>SiO^- + Me^+ = >SiOMe$ follows the order $Li^+ > K^+ > Cs^+$ for pyrogenic silica, in agreement with the increase of the surface density charge. It can be observed that our data for Q30 in LiCl 0.1 M aqueous solution, differ from those reported by Sonnenfeld et al.,[23] for fumed Aerosil 300, and Sahai and Sverjensky[45] for pyrogernic CAB-O-SIL, that is, materials formed by nonporous primary silica particles that form aggregates up to 0.5 μm in diameter, which are in equilibrium with LiCl of equal concentration. Our results, for instance, show that the surface charge increases at higher pH values than those informed by the above-mentioned authors.

However, when we compare our results with those by Salis et al.[26] for SAB15, a porous silica material with specific area 840 $m^2 \cdot g^{-1}$ and pore size 6.4 nm, we found that the surface charge density as a function of pH is rather similar. This would justify the use of the surface charge properties of the Q30 sample when analyzing the behavior of samples with smaller pores.

Moreover, it should be stressed that the reproducibility in the surface charge determinations is not very high, probably due to the difficulty in attaining equilibrium in the pH measurements, considering that diffusion in the mesoporous samples is relatively slow. Thus, this could probably explain the dispersion in all the reported results, including ours.

Diffusion of Electrolytes and Water in Confined Silica. As an example of the time evolution of the release of electrolyte from the mesoporous silica samples, determined through the conductivity measurements, the case of LiCl is illustrated in Figure 5. A rapid increase of the LiCl concentration in the bulk solution in contact with the mesoporous samples is observed at short times, followed by a long time regime, ending with a plateau which indicates that the system has attained equilibrium, that is, the chemical potential of LiCl inside the pores is equal to that of the solution, and the net flux of electrolyte is null. This figure shows that the final concentration attained in the solution at equilibrium, differs from the value estimated from the mass of electrolyte in the spheres and the amount of pure water in the conductivity cell, and that this difference depends on the pore size. This partition equilibrium effect will not be addressed here, but it is a thermodynamic aspect that does not affect the results on the dynamics of the diffusion of ions and water inside the silica pores.

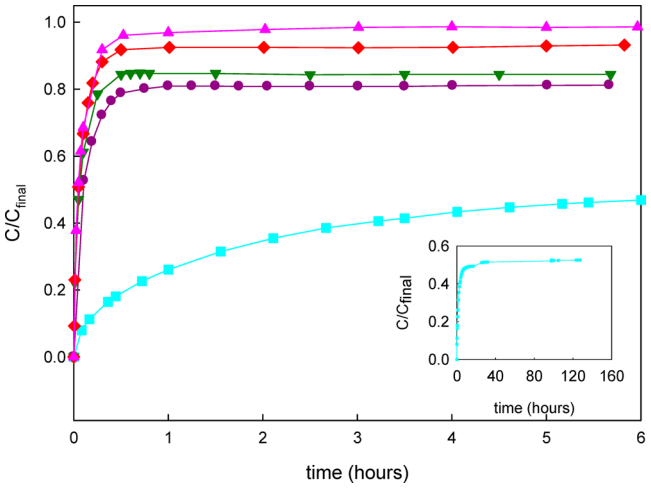

Figure 5. Time evolution of the release of LiCl from the mesoporous silica samples: (blue ■) Q3, (purple ●) Q6, (green ▼) Q10, (red ◆) Q15, and (pink ▲) Q30. The inset corresponds to the long time release from the Q3 sample. All measurements at pH = 5.2, and T = 298.15 K.

The apparent diffusion coefficients, D_p, of LiCl, KCl, and CsCl through the silica pores calculated with Eqn. 3 for the short and long times approximations are summarized in Table 2. Diffusion constants for water determined by ^{1}H NMR are also included in this table, and they correspond to water diffusion inside the pore; that is why a single diffusion coefficient is given for water.

The errors assigned to the short times calculation correspond to twice the standard deviation of the best fit of the experimental data. Errors for the long times diffusion constants were obtained considering the uncertainty in the slope of the curve of $ln\,[(1 - c(t)/c_f)(\pi^2/6)]$ vs. t. In this case, data close to the plateau were discarded for the fit since the variation of concentration with time in this region is small and, consequently, including this data in the calculations yields to large errors in D_p.

The diffusion coefficients of LiCl in the Q3 sample were determined at various pH values, while for KCl and CsCl diffusion coefficients are reported only at pH = 2.7 and 7.4 and for a limited number of samples. It should be stressed that the long time approximation could not be applied to determine the diffusion coefficient in most of the Q3 samples, since for this pore size we could not measure the concentration time dependence for $D_p t/a^2 > 0.05$.

It can be observed in Table 2 that in all cases the short times approximation gives diffusion coefficients larger than those determined with the long times approximation. This can be interpreted considering pores of ink-bottle type, where diffusion at long times is limited by the neck length scale while diffusion at short times is limited by a larger length scale, that corresponds to the pore diameter.

Figure 6 shows the short and long time diffusion coefficients of LiCl as a function of the pore or neck diameters. In this figure, D_p^s at short times are plotted as a function of the pore diameter, while D_p^l at long times are plotted as a function of the neck diameter. As it can be observed in this figure all data can be fitted with an equation of the form:

$$D = D_0[1 - e^{-bd}] \quad (6)$$

where d is the pore diameter and D_0 and b are fitting parameters, D_0 representing the diffusion coefficient for $d \rightarrow \infty$, that is, D_{bulk}. It should be stressed that a similar procedure can be applied for the other electrolytes meanwhile less pore sizes were investigated in those cases. The possibility of fitting all data with a common curve means that our assumption that the adsorption isotherm gives the pore size while the desorption isotherm gives the neck size is reasonable, being plausible to assume that the silica samples have a random distribution of pores with and without necks.

Fitting the diffusion data for LiCl at pH = 5.2 gives $D_0 = 8.29 \times 10^{-6}$ $cm^2 \cdot s^{-1}$, and $b = 0.0602$. If we consider the porosity of the material close to the average value of our samples ($\varepsilon = 0.67$) we get $D_0 = 1.24 \times 10^{-5}$ $cm^2 \cdot s^{-1}$, in very good agreement with the bulk diffusion coefficient of 0.1 M LiCl in water, $D_{bulk} = 1.27 \times 10^{-5}$ $cm^2 \cdot s^{-1}$.[27]

The diffusion constants of LiCl in the Q3 sample decrease with increasing pH, as shown in Table 2. This behavior can be explained considering that, with increasing pH the surface

DOI: 10.1021/acs.jpcc.7b11555
J. Phys. Chem. C 2018, 122, 3638−3647

Table 2. Diffusion Coefficients of Alkaline Chlorides Obtained with Equation 3 Using the Short (D_p^s) and Long Time (D_p^l) Approximations for the Confined Aqueous Electrolytes Determined at Different pHs and Restricted Diffusion Coefficients of Water (D_p) Determined by NMR with a Diffusion Time of 1 ms[a]

sample	salt	pH	D_p^s (10^6 cm^2·s^{-1})	D_p^s/D_{bulk}	D_p^l (10^6 cm^2·s^{-1})	D_p^l/D_{bulk}
Q3	LiCl	2.7	0.30 ± 0.05	0.023 ± 0.004		
Q3	LiCl	4.3	0.126 ± 0.007	0.0099 ± 0.0004		
Q3	LiCl	5.2	0.13 ± 0.01	0.0102 ± 0.0008		
Q3	LiCl	7.4	0.082 ± 0.003	0.0064 ± 0.0002		
Q6	LiCl	5.2	3.6 ± 0.2	0.28 ± 0.02	2.283 ± 0.004	0.1785 ± 0.0003
Q10	LiCl	5.2	5.7 ± 0.4	0.45 ± 0.03	3.68 ± 0.01	0.2877 ± 0.0008
Q15	LiCl	5.2	7 ± 1	0.55 ± 0.08	5.68 ± 0.03	0.444 ± 0.002
Q30	LiCl	5.2	8 ± 1	0.63 ± 0.08	7.68 ± 0.03	0.600 ± 0.002
Q3	KCl	2.7	0.64 ± 0.03	0.035 ± 0.002		
Q3	KCl	7.4	0.47 ± 0.03	0.025 ± 0.002		
Q6	KCl	7.4	5.8 ± 0.5	0.31 ± 0.03	4.31 ± 0.01	0.2337 ± 0.0005
Q30	KCl	7.4	12 ± 3	0.7 ± 0.2	12 ± 3	0.7 ± 0.2
Q3	CsCl	2.7	0.97 ± 0.07	0.052 ± 0.004		
Q3	CsCl	7.4	0.78 ± 0.03	0.042 ± 0.002	0.710 ± 0.003	0.0379 ± 0.0002
Q30	CsCl	7.4	9.5 ± 0.8	0.51 ± 0.04	8.62 ± 0.03	0.461 ± 0.002

sample	solvent	pH	D_p (10^6 cm^2·s^{-1})	D_p/D_{bulk}
Q3	H_2O	5.2	1.20 ± 0.06	0.050 ± 0.004
Q6	H_2O	5.2	9.5 ± 0.5	0.40 ± 0.03
Q10	H_2O	5.2	12.7 ± 0.7	0.54 ± 0.04
Q15	H_2O	5.2	14.5 ± 0.7	0.61 ± 0.04
Q30	H_2O	5.2	14.8 ± 0.7	0.63 ± 0.04

[a]All values correspond to 298.15 K.

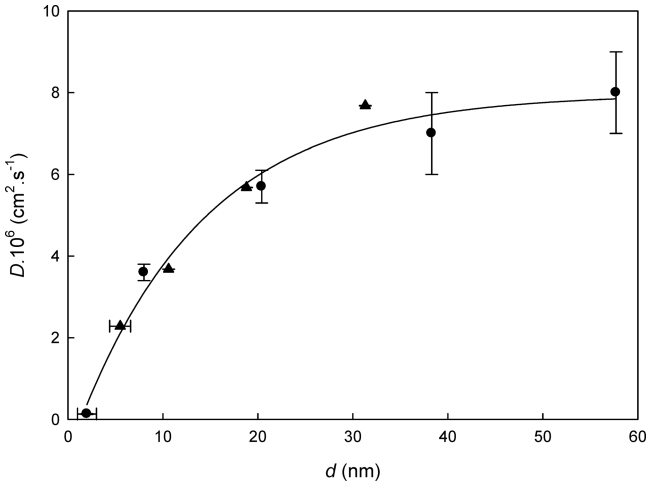

Figure 6. D_p of LiCl as a function of pore diameter (●), and as a function of the diameter of the necks (▲). The bold line corresponds to the fit of all data performed with eq 6, with $D_0 = 8.29 \times 10^{-6}$, and $b = 0.0602$. pH = 5.2, and $T = 298.15$ K.

negative charge density increases. Thus, the interaction of Li^+ ions with the pore walls increases, and the Li^+ ion diffusion, and consequently the diffusion of the salt, is slow down. The same dependence of D_p with pH can be observed for KCl and CsCl salts, although less pH values were analyzed in these cases.

In porous media it is common to express the apparent diffusion coefficient as

$$D_p = \frac{\varepsilon D_{bulk}}{\tau} \tag{7}$$

where D_{bulk} is the diffusion constant of the electrolyte in the aqueous bulk solution, ε is the material porosity, and τ is a dimensionless parameter called pore tortuosity ($\tau > 1$), that accounts for the real length of the pores compared to an ideal linear pore. Other factors that affect the diffusion constant in the pores, such as interactions of the solute with the pore surface, are incorporated in the tortuosity factor. Therefore, τ can be called "apparent tortuosity".[17]

Table 2 shows the ratio between the diffusion constant in the pore and in the bulk, which is equal to ε/τ. The diffusion coefficients of the bulk 0.1 M alkaline chlorides aqueous solutions were obtained from Robinson and Stokes.[27] The bulk diffusion coefficient of water was obtained from data reported by Holtz et al.,[46] and Mills.[47]

Figure 7 shows the tortuosity factors for all studied electrolytes and water as a function of pore size, calculated with the porosity factors taken from Table 1. In this figure we plotted τ, given by D_p^s and D_p^l, as a function of pore and neck sizes, respectively. For the case of water, τ is plotted as a function of the pore diameter since diffusion by NMR measurements is analyzed in the interior of the pore.

A similar trend can be observed for all studied solutes, that is, a monotonic slight increase in tortuosity with decreasing pore size for $d > 5$ nm, while τ increases markedly with decreasing pore size for $d < 5$ nm. In Figure 7 one can clearly observe that the tortuosity coefficients for the sample Q3, with pore sizes around 2 nm, are much higher that for the rest of the samples, and the differences between cations becomes evident. The order of tortuosity indicates that the interaction of Li^+ ions with the silanol groups on the pore wall is higher than that of K^+ and Cs^+ ions, while the tortuosity for the diffusion of water is lower than those observed for the ionic species. It should be emphasized that even when the tortuosity was measured for the diffusion of LiCl, KCl, and CsCl inside the mesopores, the effect is mainly due to the cations that interact with the ionizable silanol groups, while the common Cl^- anion only plays a secondary role.

DOI: 10.1021/acs.jpcc.7b11555
J. Phys. Chem. C 2018, 122, 3638−3647

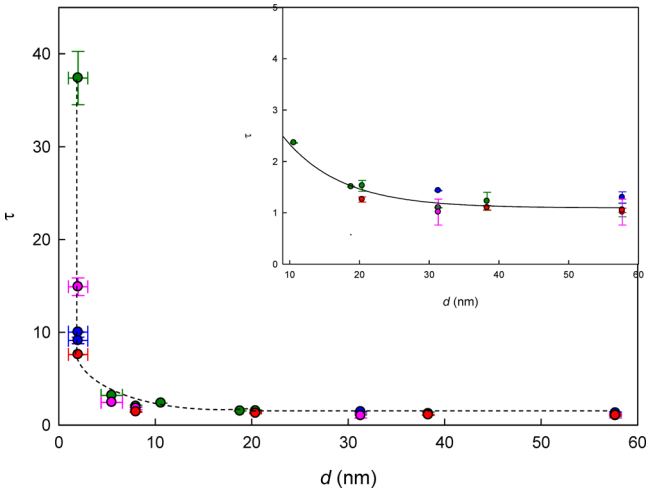

Figure 7. Tortuosity coefficients for (green ●) LiCl, (pink ●) KCl, (blue ●) CsCl, and (red ●) water as a function of pore size. The inset corresponds to torturosity data for $d \geq 10$ nm. LiCl data at pH = 5.2, KCl and CsCl at pH = 7.4. All measurements were performed at 298.15 K.

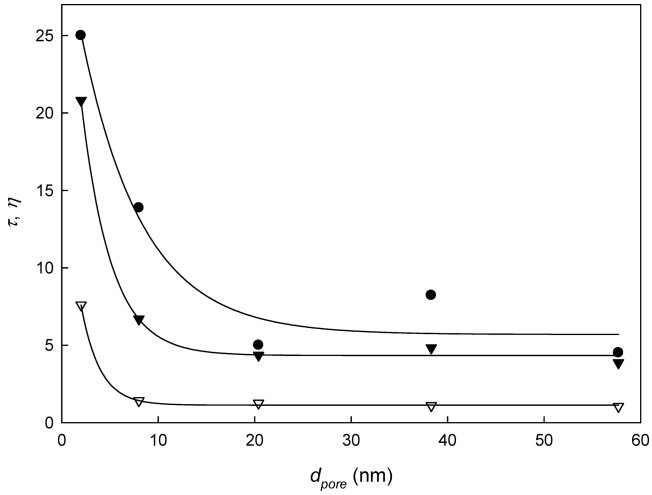

Figure 8. Coefficients τ for ^{1}H of water (▽), and η for Li^+ (●) and ^{1}H of water (▼), as a function of pore diameter. pH = 5.2, T = 298.15 K.

For samples with large pores, like Q30, the diffusion inside the pore is less restricted by interactions with the pore walls and, for this reason, the differences between the diffusion coefficients in the pore and the bulk is given by the porosity factor. Thus, in these samples it is reasonable to observe that $D_p^s \approx D_p^l$ for all electrolytes (see Table 2).

A similar dependence of tortuosity with pore diameter was reported by Takahashi et al.[17] These authors studied the diffusion of nickel nitrate dissolved in water in porous silica plates of different pore sizes, ranging from 2 to 17 nm, by means of absorbance measurements. They observed that $\tau \approx 1$ for pores with diameters above 5 nm, while this value increases drastically for smaller pores. The difference with our results for alkaline cations, where $\tau \approx 1$ for pores larger than 20−30 nm, is probably due to the strong hydration of Ni^{2+} ions which reduces the electrostatic interactions with the silanol groups on the pore wall. It is also possible that distinctive pore geometries (plates vs cylinders) play a role in the observed different behavior.

Spin−Lattice Relaxation Time of Water and Lithium Ion. In analogy with the definition of τ, and as suggested by D'agostino et al.,[2] we define the parameter η as,

$$\eta = \frac{T_{1,bulk}}{T_{1,p}} \tag{8}$$

where $T_{1,bulk}$ and $T_{1,p}$ are the NMR spin−lattice relaxation times in the bulk and within the pores, respectively, which can be measured for Li^+ ion or water protons (^{1}H). As ^{7}Li has a spin 3/2, the NMR relaxation is governed by the interaction between its nuclear electric quadrupole moment and the local electric field gradient (EFG), and the measurement of the relaxation times provides information regarding the molecular motions through the modulation of the quadrupolar interaction.

Recently Mitchell and Fordham,[48] and Kausik et al.[49] showed that the usual framework that describes dipolar driven relaxation under confinement, which is based on the Brownstein and Tarr model,[50] cannot be directly applied for ^{23}Na in confined NaCl brine, whereas the modulation of the EFG must be taken into account to probe the restricted dynamics. Following the recommended procedure we obtained, to the best of our knowledge, the first relaxation results of quadrupolar ^{7}Li under confinement in mesoporous systems.

As it can be observed in Figure 8, the trend of η for ^{7}Li and ^{1}H as a function of the pore size is the same as that observed for τ derived from the measured diffusion coefficients of ^{1}H and alkaline chlorides. In the case of ^{1}H the interpretation is straightforward: water/surface interactions reduce both the translational mobility and molecular reorientations. The behavior observed for Li^+ ions may be a consequence of both, a reduction in the molecular reorientations of the ion given by the interactions with the water molecules with reduced mobility, and by the formation of SiO^-Li^+ pairs

In the case of diffusion, the characteristic length for molecular displacements is $l_D = \sqrt{D_{bulk}\tau_2} = 1.5$ μm. The ratio between the diffusion length and the pore diameter gives a measure of the average of excursions that a molecule undergoes within the pore during the measurement time, which for the larger pores is around 50, while for the smallest one is around 500. This would explain why only a small restriction in molecular mobility is observed for pores larger than 20 nm ($\tau \sim 1.6$), while $\tau \approx 8$ for the smaller pores. Since the relaxation times are sensitive to the local environment, the fact that η increases as the pores size decreases reveals that this trend is due to short-range interactions. In fact this mechanism seems to be more sensitive than self-diffusion, with values of $\eta \approx 4$ for both water and lithium in pores larger than 10 nm. On the other hand, the results for the smallest pore are comparable for both techniques.

CONCLUSIONS

The diffusion of water and alkaline chlorides has been studied in mesoporous silica with pore sizes ranging from 2 nm up to more than 30 nm. The morphology of the silica samples changes from a microporous structure for the Q3 sample, an interconnected network of pores (cage-like) for the Q6 sample, and typical mesoporous materials with ink-bottle pores for the rest. The porosity of the samples increases with increasing pore size, reaching a constant value for the samples with larger pores, while the surface area decreases monotonically with increasing pore size.

DOI: 10.1021/acs.jpcc.7b11555
J. Phys. Chem. C 2018, 122, 3638−3647

The release of electrolytes from the spherical samples as a function of time exhibits two differentiated regimes, at short and long times, which correlate quite well with the size of the pores and necks. The diffusion of water inside the pores, as determined by ^{1}H NMR, follows the same trend with pore size than the diffusion of electrolytes, meaning that there is some coupling between the ions and water diffusional mobilities, particularly for silica samples with large pores. In the microporous sample (Q3) the tortuosity for Li^+ ion diffusion is much larger than for water diffusion, as a consequence of the electrostatic interaction of the ion with the ionizable silanol groups on the pore wall. The spin−lattice relaxation time measurements of ^{1}H-water and Li^+ ions confirm the above-mentioned behavior, reinforcing the idea that the increase of the tortuosity coefficient due to confinement effects are important for mesoporous silica with pore sizes below 5 nm. These confinement effects are particularly strong for micropores (pore sizes around 2 nm) and they could be associated with interactions of water with silanol groups (*i.e.* through hydrogen bonding), and the electrostatic interaction of the alkaline ions with the ionizable silanol groups. The tortuosity coefficient determined for the microporous sample (Q3) for the different alkaline cations seems to indicate that this interaction increases in the order $Cs^+ < K^+ < Li^+$, while water mobility would be hindered by the pore surface through weaker hydrogen bond interactions.

A more detailed study of the interactions of different ions (having different charge/size ratios), and other hydrogen bonding neutral solutes with silica surfaces is mandatory for a complete understanding of the tortuosity effect in these mesoporous materials. A forthcoming work will deal with this important issue.

■ ASSOCIATED CONTENT

Supporting Information

The Supporting Information is available free of charge on the ACS Publications website at DOI: 10.1021/acs.jpcc.7b11555.

Surface charge density as a function of pH for CARIACT Q30 (PDF)

■ AUTHOR INFORMATION

Corresponding Authors

*(H.R.C.) E-mail: hrcorti@cnea.gov.ar.
*(M.P.L.) E-mail: longinot@qi.fcen.uba.ar.

ORCID

M. Paula Longinotti: 0000-0001-8221-1933

Present Address

[⊥]Department of Chemistry, Universidad Nacional de Río Cuarto-CONICET, Ruta 8 y 36 Km 601, Río Cuarto, Córdoba, Argentina.

Author Contributions

D.C.M.C. performed the electrolytes diffusion measurements. M.M.B. measured and analyzed the adsorption and desorption isotherms. F.V.C. and R.H.A. performed the RMN measurements and analysis. M.P.L. and H.R.C. designed the experiments, analyzed the results and wrote the manuscript.

Notes

The authors declare no competing financial interest.

■ ACKNOWLEDGMENTS

The authors express thanks for the financial support of ANPCyT-FONCyT (PICT 2013 No. 1818 and No. 2238). M.P.L., M.M.B., F.V.C., R.H.A., and H.R.C. are members of CONICET. R.H.A. and F.V.C. thank the Universidad Nacional de Córdoba (UNC) for financial support. D.C.M.C. expresses thanks for a postdoctoral fellowship from CONICET.

■ REFERENCES

(1) Hansen, E. W.; Schmidt, R.; Stöcker, M.; Akporiaye, D. Self-diffusion coefficient of water in mesoporous MCM-41 materials determined by ^{1}H nuclear magnetic resonance spin-echo measurements. *Microporous Mater.* **1995**, *5*, 143−150.

(2) D'Agostino, C.; Mitchell, J.; Gladden, L. F.; Mantle, M. D. Hydrogen Bonding Network Disruption in mesoporous catalyst supports probed by PFG-NMR diffusometry and NMR relaxometry. *J. Phys. Chem. C* **2012**, *116*, 8975−8982.

(3) Kiwilsza, A.; Pajzderska, A.; Gonzalez, M. A.; Mielcarek, J.; Wąsicki, J. QENS and RMN study of water dynamics in SBA-15 with a low water content. *J. Phys. Chem. C* **2015**, *119*, 16578−16586.

(4) Takahara, S.; Sumiyama, N.; Kittaka, S.; Yamaguchi, T.; Bellissent-Funel, M. C. Neutron scattering study on dynamics of water molecules in MCM-41. 2. Determination of translational diffusion coefficient. *J. Phys. Chem. B* **2005**, *109*, 11231−11239.

(5) Mamontov, E.; Cole, D. R.; Dai, S.; Pawel, M. D.; Liang, C. D.; Jenkins, T.; Gasparovic, G.; Kintzel, E. Dynamics of water in LiCl and $CaCl_2$ aqueous solutions confined in silica matrices: A backscattering neutron spectroscopy study. *Chem. Phys.* **2008**, *352*, 117−124.

(6) Bourg, I. C.; Steefel, C. I. Molecular dynamics simulations of water structure and diffusion in silica nanorpores. *J. Phys. Chem. C* **2012**, *116*, 11556−11564.

(7) Argyris, D.; Cole, D. R.; Striolo, A. Ion-specific effects under confinement: the role of interfacial water. *ACS Nano* **2010**, *4*, 2035−2042.

(8) Ho, T. A.; Argyris, D.; Cole, D. R.; Striolo, A. Aqueous NaCl and CsCl solutions confined in crystalline slit-shaped silica nanopores of varying degree of protonation. *Langmuir* **2012**, *28*, 1256−1266.

(9) Bonnaud, P. A.; Coasne, B.; Pellenq, J. − M. Solvated calcium ions in charged silica nanopores. *J. Chem. Phys.* **2012**, *137*, 064706.

(10) Gonzalez Solveyra, E.; de la Llave, E.; Molinero, V.; Soler Illia, G. J. A. A.; Scherlis, D. A. Structure, dynamics, and phase behavior of water in TiO_2 nanopores. *J. Phys. Chem. C* **2013**, *117*, 3330−3342.

(11) Renou, R.; Szymczyk, A.; Ghoufi, A. Water confinement in nanoporous silica materials. *J. Chem. Phys.* **2014**, *140*, 044704.

(12) Renou, R.; Szymczyk, A.; Ghoufi, A. Ultraconfinement of aqueous electrolytic solutions within hydrophilic nanotubes. *RSC Adv.* **2014**, *4*, 32755−32761.

(13) Videla, P. E.; Sala, J.; Martí, J.; Guardia, E.; Laria, D. Aqueous electrolytes confined within functionalized silica nanopores. *J. Chem. Phys.* **2011**, *135*, 104503.

(14) Thompson, H.; Soper, A. K.; Ricci, M. A.; Bruni, F.; Skipper, N. T. The three-dimensional structure of water confined in nanoporous Vycor glass. *J. Phys. Chem. B* **2007**, *111*, 5610−5620.

(15) Zhu, H.; Ghoufi, A.; Szymczyk, A.; Balannec, B.; Morineau, D. Computation of the hindrance factor for the diffusion for nano-confined ions: molecular dynamics simulations versus continuum-based models. *Mol. Phys.* **2012**, *110*, 1107−1114.

(16) Balme, S.; Picaud, F.; Manghi, M.; Palmeri, J.; Bechelany, M.; Cabello-Aguilar, S.; Abou-Chaaya, A.; Miele, P.; Balanzat, E.; Janot, J. M. Ionic transport through sub-10 nm diameter hydrophobic high-aspect ratio nanopores: experiment, theory and simulation. *Sci. Rep.* **2015**, *5*, 10135.

(17) Takahashi, R.; Sato, S.; Sodesawa, T.; Nishida, H. Effect of pore size on the liquid-phase pore diffusion of niquel nitrate. *Phys. Chem. Chem. Phys.* **2002**, *4*, 3800−3805.

(18) Kunetz, J.; Hench, L. Restricted diffusion of chromium nitrate salt solutions into porous sol-gel silica monoliths. *J. Am. Ceram. Soc.* **1998**, *81*, 877−884.

DOI: 10.1021/acs.jpcc.7b11555
J. Phys. Chem. C 2018, 122, 3638−3647

(19) Koone, N. D.; Guo, J. D.; Zerda, T. W. Diffusion of Er^{3+} in porous sol-gel glass. *J. Non-Cryst. Solids* **1997**, *211*, 150−157.
(20) http://www.fujisilysia.com/products/cariact/.
(21) Barrett, E. P.; Joyner, L. G.; Halenda, P. P. The determination of pore volume in porous substances. I. Computations from nitrogen isotherms. *J. Am. Chem. Soc.* **1951**, *73*, 373−380.
(22) Broekhoff, J. C. P.; de Broer, J. H. Studies on pore systems in catalysis. XII. Pore distributions from the desorption branch of a nitrogen sorption isotherm in the case of cylindrical pores A. An analysis of the capillary evaporation process. *J. Catal.* **1968**, *10*, 368−376.
(23) Sonnefeld, J.; Göbel, A.; Vogelsberger, W. Surface charge density on spherical silica particles in aqueous alkali chloride solutions. Part 1. Experimental results. *Colloid Polym. Sci.* **1995**, *273*, 926−931.
(24) Sonnefeld, J.; Löbbus, M.; Vogelsberger, W. Determination of electric double layer parameters for spherical silica particles under application of the triple layer model using surface charge density data and results of electrokinetic sonic amplitude measurements. *Colloids Surf., A* **2001**, *195*, 215−225.
(25) Dove, P. M.; Craven, C. M. Surface charge density on silica in alkali and alkaline earth chloride electrolyte solutions. *Geochim. Cosmochim. Acta* **2005**, *69*, 4963−4970.
(26) Salis, A.; Parsons, D. F.; Boström, M.; Medda, L.; Barse, B.; et al. Ion specific surface charge density of SBA-15 mesoporous silica. *Langmuir* **2010**, *26*, 2484−2490.
(27) Robinson, R. A.; Stokes, R. H. *Electrolyte Solutions*; Butterworths Scientific Pub.: London, 1955; Appendix 6.1, p 452.
(28) Wu, Y. C.; Koch, W. K.; Hamer, W. J.; Kay, R. L. Review of electrolytic conductance standards. *J. Solution Chem.* **1987**, *16*, 985−997.
(29) Grathwohl, P. *Diffusion in natural porous media: contaminant transport, sorption/ desorption and dissolution kinetics*; Springer: New York, 1998.
(30) Crank, J. *The Mathematics of Diffusion*; Clarendox Press: Oxford, U.K., 1976; p 91.
(31) Carr, H.; Purcell, E. M. Effects of Diffusion on Free Precession in Nuclear Magnetic Resonance Experiments. *Phys. Rev.* **1954**, *94*, 630−638.
(32) Meiboom, S.; Gill, D. Modified Spin-Echo Method for Measuring Nuclear Relaxation Times. *Rev. Sci. Instrum.* **1958**, *29*, 688−691.
(33) Casanova, F.; Perlo, J.; Blümich, B. *Single-Sided NMR*; Springer: New York, 2011.
(34) BP Chemical Limited. Supported heteropolyacid catalysts. Patent EP 1982761 A1, published October 22, 2008.
(35) Hamasaka, G.; Kawamorita, S.; Ochida, A.; Akiyama, R.; Hara, K.; Fukuoka, A.; Asakura, K.; Chun, W. J.; Ohmiya, H.; Sawamura, M. Synthesis of silica-supported compact phosphines and their application to rhodium-catalyzed hydrosilylation of hindered ketones with triorganosilanes. *Organometallics* **2008**, *27*, 6495−6506.
(36) Yang, G.; Wang, D.; Yoneyama, Y.; Tan, Y.; Tsubaki, N. Facile synthesis of H-type zeolite shell on a silica substrate for tandem catalysis. *Chem. Commun.* **2012**, *48*, 1263−1265.
(37) Thommes, M.; Kaneko, K.; Neimark, A. V.; Olivier, J. P.; Rodriguez-Reinoso, F.; Rouquerol, J.; Sing, K. S. W. Physisorption of gases, with special reference to the evaluation of surface area and pore size distribution (IUPAC Technical Report). *Pure Appl. Chem.* **2015**, *87*, 1051−1069.
(38) Grosman, A.; Ortega, C. Capillary condensation in porous materials. Hysteresis and interaction mechanism without pore blocking/percolation process. *Langmuir* **2008**, *24*, 3977−3986.
(39) Rouquerol, F.; Rouquerol, J.; Sing, K. *Adsorption by powders and porous solids. Principles, Methodology and Applications*; Academic Press: London, 1999.
(40) Groen, J. C.; Pérez-Ramírez, J. Critical appraisal of mesopore characterization by adsorption analysis. *Appl. Catal., A* **2004**, *268*, 121−125.
(41) Fu, Q.; Bao, X. Surface chemistry and catalysis confined under two-dimensional materials. *Chem. Soc. Rev.* **2017**, *46*, 1842−1874.
(42) Fan, J.; Yu, C.; Gao, F.; Lei, J.; Tian, B.; Wang, L.; Luo, Q.; Tu, B.; Zhou, W.; Zhao, D. Cubic mesoporous silica with large controllable entrance sizes and advanced adsorption properties. *Angew. Chem., Int. Ed.* **2003**, *42*, 3146−3150.
(43) Cychosz, K. A.; Guillet-Nicolas, R.; García-Martínez, J.; Thommes, M. Recent advances in the textural characterization of hierarchically nanoporous materials. *Chem. Soc. Rev.* **2017**, *46*, 389−414.
(44) Kruk, M.; Jaroniec, M. Argon adsorption at 77 K as a useful tool for the elucidation of pore connectivity in ordered materials with large cagelike mesopores. *Chem. Mater.* **2003**, *15*, 2942−2949.
(45) Sahai, N.; Sverjensky, D. A. Evaluation of internally consistent parameters for the triple-layer model by the systematic analysis of oxide surface titration data. *Geochim. Cosmochim. Acta* **1997**, *61*, 2801−2826.
(46) Holz, M.; Heil, S. R.; Sacco, A. Temperature-dependence self-diffusion coefficients of water and six selected molecular liquids for calibration in accurate 1H NMR PFG measurements. *Phys. Chem. Chem. Phys.* **2000**, *2*, 4740−4742.
(47) Mills, R. Self-diffusion in normal and heavy water in the range 1−45 °C. *J. Phys. Chem.* **1973**, *77*, 685−688.
(48) Mitchell, J.; Fordham, E. J. Sodium-23 NMR in porous media. *Microporous Mesoporous Mater.* **2017**, DOI: 10.1016/j.micromeso.2017.02.004.
(49) Kausik, R.; Fellah, K.; Yang, D. M. Sodium NMR relaxation in mesoporous systems. *Microporous Mesoporous Mater.* **2017**, DOI: 10.1016/j.micromeso.2017.03.009.
(50) Brownstein, K. R.; Tarr, C. E. Spin lattice relaxation in a system governed by diffusion. *J. Magn. Reson.* **1977**, *26*, 17−24.

DOI: 10.1021/acs.jpcc.7b11555
J. Phys. Chem. C 2018, 122, 3638−3647